Reflections Regarding Recent Rotary Rig Results

L. E. Ericsson*
Lockheed Missiles & Space Company Inc., Sunnyvale, California

Recent rotary rig experiments are examined to evaluate how well they stimulate dynamic conditions existing in full-scale flight. It is found that most rig designs used are prone to cause significant interference with the vortex wake shed from an advanced aircraft at high angles of attack. The support interference problem can be aggravated substantially by coupling existing in the critical Reynolds number range between vehicle motion and boundary-layer transition, a coupling unlikely to have been simulated in most wind-tunnel tests.

Nomenclature

A = cross-sectional area
b = wingspan
c = mean aerodynamic chord
c_0 = maximum wing chord
d = body diameter
l = rolling moment; coefficient $C_l = l/(\rho V^2/2)Sb$
M = freestream Mach number
n = yawing moment; coefficient $C_n = n/(\rho V^2/2)Sb$
N = normal force; coefficient $C_N = N/(\rho V^2/2)\pi d^2/4$
p = pressure; coefficient $C_p = (p - p_\infty)/(\rho V^2/2)$
r = corner radius
Re = Reynolds number, $= Vc/\nu$; $R_w = Vw/\nu$
S = reference area, effective wing area
V = freestream velocity
w = cross-sectional width
x = chordwise distance from leading edge
y = body side force; coefficient $c_y = y/(\rho V^2/2)A$
Y = side force; coefficient $C_y = Y/(\rho V^2/2)S$
α = angle of attack
β = angle of sideslip ($\beta = 0$ for experimental results shown)
ν = kinematic viscosity of freestream
ρ = density of freestream
ϕ = coning angle, angle of roll of rotary rig around its axis
ω = coning rate, $= \partial\phi/\partial t$

Subscripts

s = sting support
w = body width
∞ = freestream condition

Introduction

STEADILY increasing performance demands expose present-day aircraft and aerospace vehicles to unsteady flowfields, which generate highly nonlinear aerodynamics that exhibit strong coupling between longitudinal and lateral degrees of freedom. The complex vehicle dynamics are caused by separated flow effects of various types, which have largely eluded theoretical description and, therefore, are placing great demands on dynamic testing capabilities.[1] One very important experimental tool for obtaining needed information about dynamic cross-coupling effects is the rotary rig.

Received March 7, 1986, revision received Aug. 4, 1986.

*Senior Consulting Engineer. Fellow AIAA.

As the vortex asymmetry, resulting at high angles of attack, leaves one vortex close to the fuselage[2] (Fig. 1), one has to be concerned about support interference effects.[3] This problem is aggravated by the inboard movement of the lower vortex, as reflected in the vortex-induced aerodynamic loads[4,5] (Fig. 2). In difference to what occurs on a delta wing, where the flow separation is fixed, the vortex asymmetry results in an increase rather than a decrease of the normal force.[6] The inboard movement of the flow separation and the associated body vortex has been documented by flowfield measurements.[7]

In addition to support interference one faces the usual problem of Reynolds number scaling, which becomes especially difficult in the case of dynamic tests.[8] Recent rotary rig results are used to illustrate the abovementioned difficulties when using subscale dynamic test data for prediction of the high-α vehicle dynamics of advanced aircraft.

Discussion

Recently, an effort has been made to find out more about support interference effects at high angles of attack. Malcolm[9] tested a model of the F-15 aircraft using a sting support mounted at different angles (α_s) relative to the fuselage (Fig. 3). Figures 1 and 3 indicate that one could expect sting-support interference to be different for $\alpha_s = 45$ and 70 deg. For $\beta = 0$, the α range 40 deg $< \alpha <$ 75 deg could be tested with both sting-support arrangements (Fig. 4). As expected, the support interference differs for the two α_s values, both in static and dynamic tests (Figs. 5 and 6, respectively). The difference is especially large for the nose-boom-on case. Why?

Reference 10 discusses how the nose boom acts similarly to nose bluntness, delaying the formation of asymmetric vortices. Thus, the nose-boom-on configuration will retain a

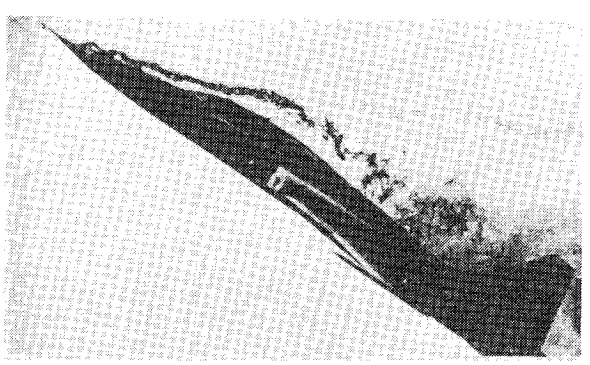

Fig. 1 Asymmetric vortex shedding from the slender nose of an advanced aircraft at $\alpha = 40$ deg and $\beta = 0$.[2]

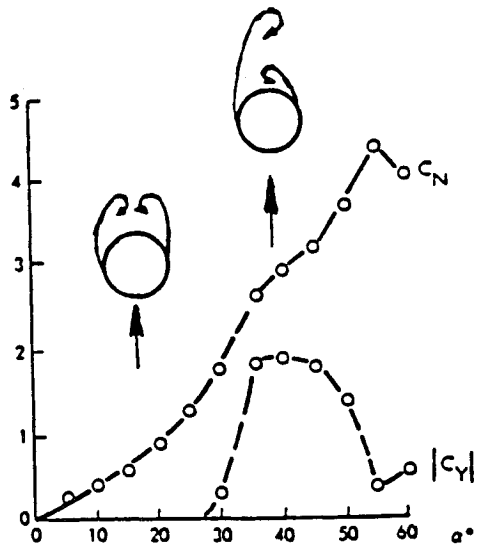

Fig. 2 Vortex-induced effects on $C_n(\alpha)$ and $C_y(\alpha)$ of a tangent-ogive at $\beta = 0$.[5]

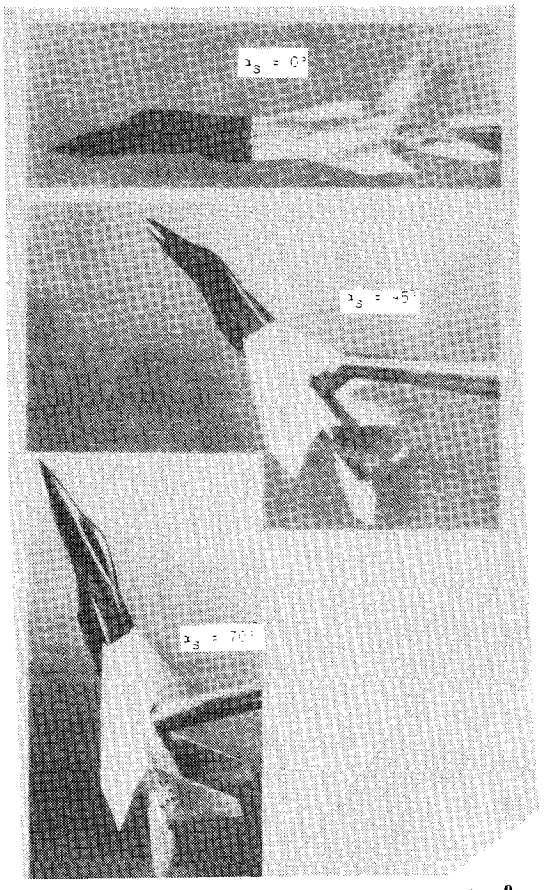

Fig. 3 Support system for high incidence testing.[9]

single asymmetric vortex pair to higher α than the nose-boom-off configuration, thereby producing a larger potential for support interference. Another consequence is that the unsteady asymmetric vortex shedding of the Kármán type, which usually starts to occur at angles of attack above $\alpha = 60$ deg for pointed nose geometries, will be delayed to higher α. The experimental results[9] in Fig. 7 show that at $\alpha = 70$ deg the nose-boom-off configuration has unsteady Kármán-type asymmetric vortex shedding,[11] with the asymmetry flipping back and forth, producing no vortex-induced net side force.

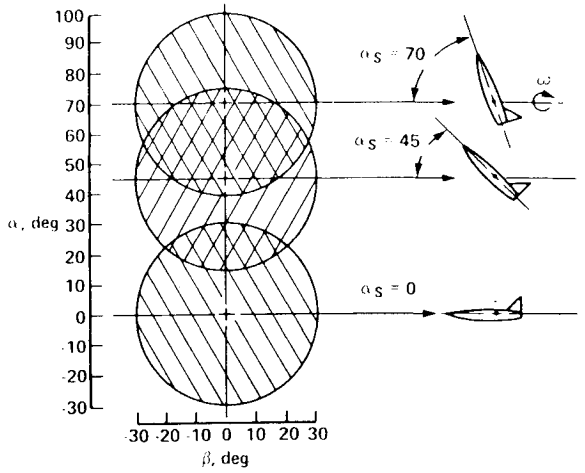

Fig. 4 (α,β) range for different sting-support angles α_s.[9]

As a consequence, there is no support interference, and the C_n variation with the dimensionless coning rate $\omega b/2V$ is more or less linear without any zero offset at zero spin rate. In contrast, the nose-boom-on configuration maintains steady asymmetric vortex shedding at $\alpha = 70$ deg, resulting in large vortex-induced effects on C_n, with associated zero offset at zero spin rate. The presence of stationary asymmetric vortices produces the potential for support interference, as illustrated by the effect of α_s shown in Fig. 6.

The results in Fig. 6 for the nose-boom-on configuration at $Re = 1.54 \times 10^6$ indicate that the C_n characteristics follow two different zero-offset $(\omega b/2V)$ branches for positive and negative coning rates. Why? Some hysteresis may be expected even without support interference, based on past experience with separated flow. However, the α_s effect shown in Fig. 6 demonstrates that the support strongly affects this coning rate hysteresis. It is easy to see why. The coning-induced sidewash at the nose affects the vortex formation similarly to the sidewash generated by sideslip, biasing both symmetric and asymmetric vortices. Because it is very difficult for the vortex to impinge on the sting in a biased, off-center position and stay on the sting, the vortex will always jump between the two possible offset positions relative to the sting, thereby enlarging any hysteresis present without support interference or creating hysteresis where none would otherwise have existed.

The results in Fig. 5 for the static case indicate that even when the vortex impinges at the center of the sting, it will jump to one of the two extreme positions. The results for the nose-boom-on case at $Re = 4 \times 10^6$ show further that which one of the two alternate states the vortex chooses can be influenced by the support. Once the biased position has been selected, it is difficult to get the vortex to flip to the opposite position.

Figure 8 shows that for the nose-boom-off case, the offset characteristics are established only for $\alpha_s = 50$ and $\alpha_s = 60$ deg, not for $\alpha_s = 70$, 80, and 90 deg, because no steady asymmetric vortex shedding can be established for these angles. Likewise, when the Reynolds number is increased so that supercritical crossflow conditions are established with corresponding negligibly small vortex-induced asymmetric loads,[12] the sting-support interference disappears ($Re \geq 4.0 \times 10^6$ in Fig. 9).

That a leeside strut or sting will cause a large interference with the vortex wake from a slender body at high angles of attack has been demonstrated[13] (Fig. 10). According to Hummel's results[14] (Fig. 11), one would also expect an interaction between shed body vortices and a downstream sting-strut geometry.

For a typical rotary rig geometry, such as the one[15] shown in Fig. 12, the vortex interference will occur with the cranked sting part. It may not be possible to build a rig that has enough

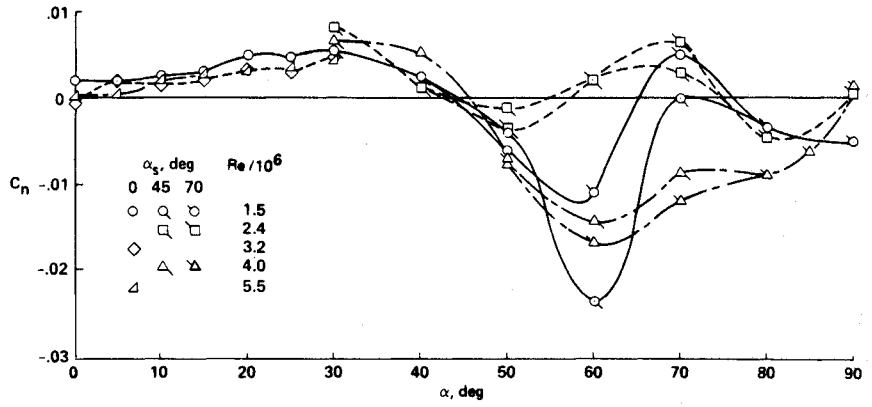

a) Nose boom off.

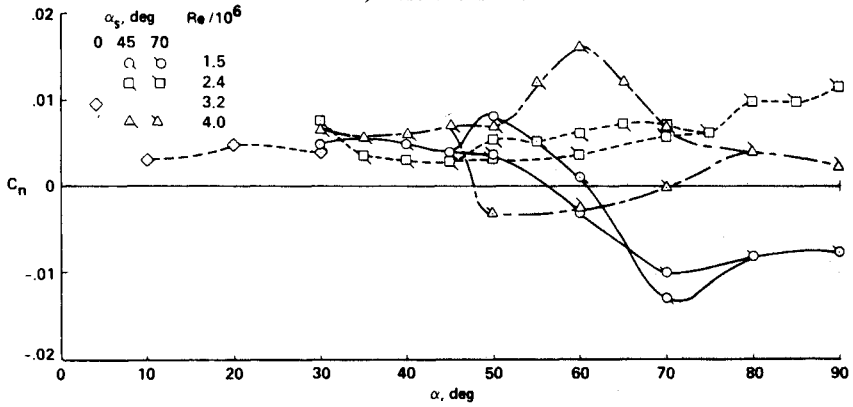

b) Nose boom on.

Fig. 5 Effect of support incidence α_s on static C_n characteristics.[9]

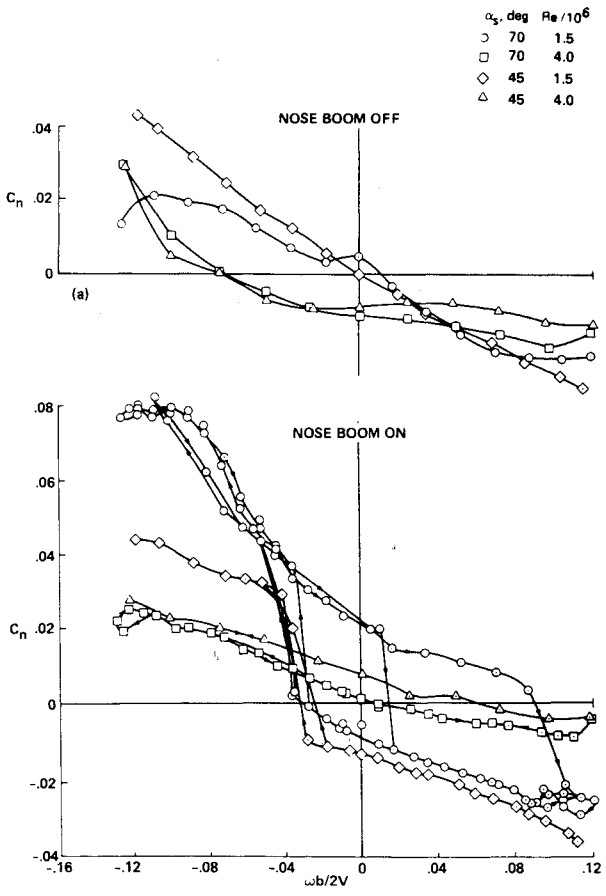

Fig. 6 Effect of support incidence α_s on dynamic C_n characteristics at $\alpha = 70$ deg.[9]

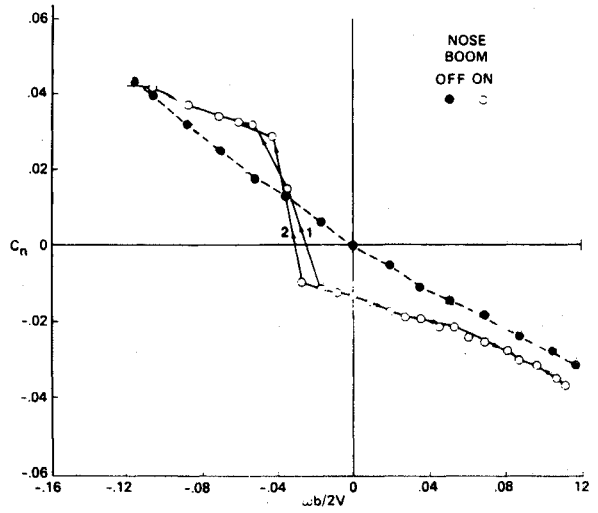

Fig. 7 Effect of nose boom on dynamic C_n characteristics at $\alpha_s = 45$ deg, $\alpha = 70$ deg, and $Re = 1.5 \times 10^6$.[9]

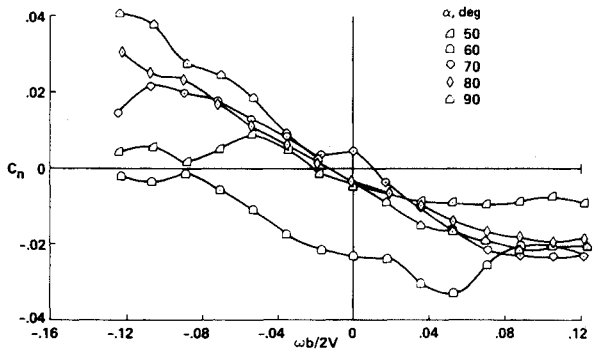

Fig. 8 Effect of angle of attack on dynamic C_n characteristics for nose boom off at $Re = 1.5 \times 10^6$.[9]

distance between the model nose and the drive mechanism to cause the asymmetric vortex to miss the cranked sting for the coning rates of practical interest. It may, however, be possible to correct for support interference, using combined static and dynamic tests, as its discussed in Ref. 16.

The test results for a high incidence research model (HIRM), using the rotary rig shown in Fig. 13, show evidence of support intereference at 40-deg angle of attack[17] (Fig. 14). According to the authors, static tests[18] have shown that at $\alpha = 40$ deg (and $\beta = 0$) side forces and yawing moments are generated by asymmetric vortices shed from the nose. Furthermore, the magnitude of the asymmetric loads was substantially larger in the dynamic test (Fig. 14c) than in

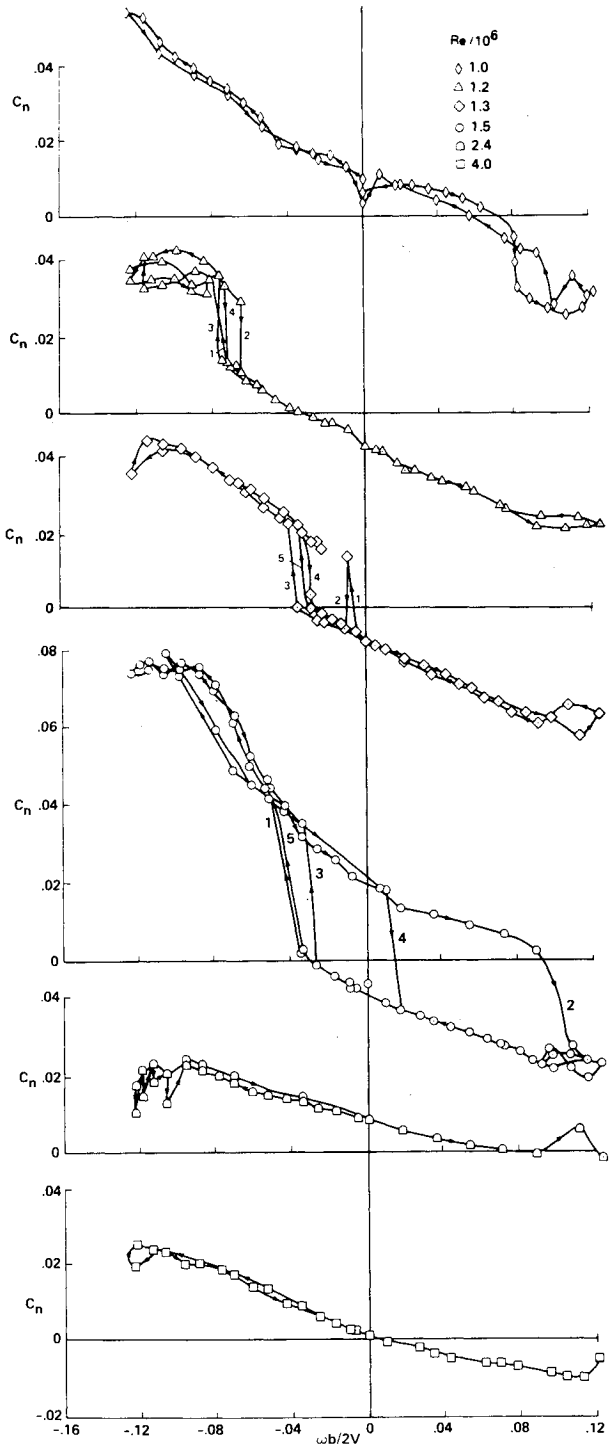

Fig. 9 Effect of Reynolds number on dynamic C_n characteristics for nose boom on at $\alpha_s = 70$ deg.[9]

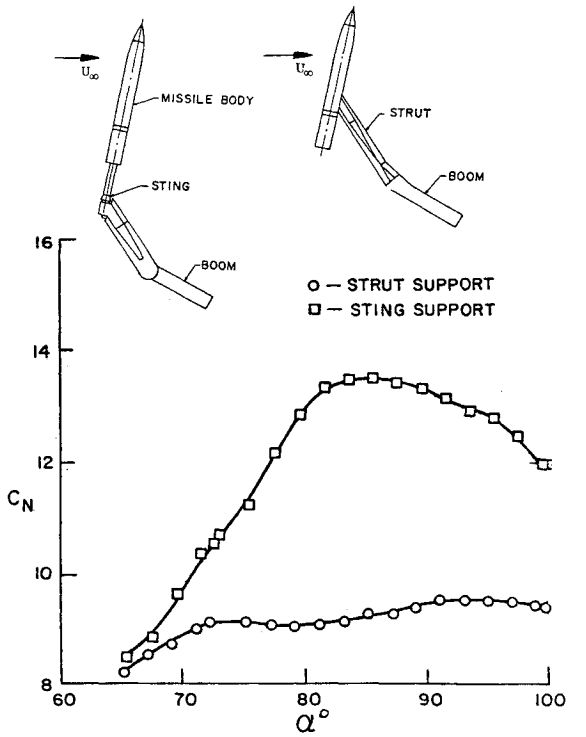

Fig. 10 Effect of strut support on ogive-cylinder static characteristics.[13]

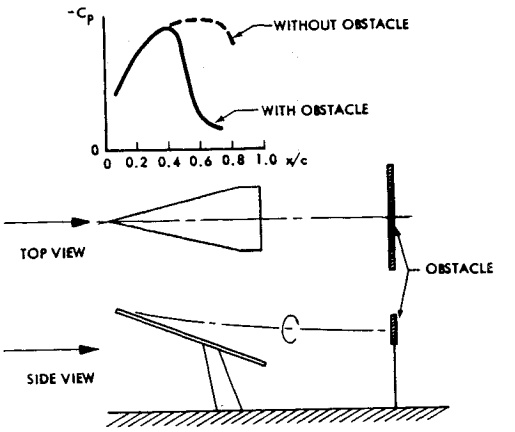

Fig. 11 Vortex bursting caused by downstream obstacle.[14]

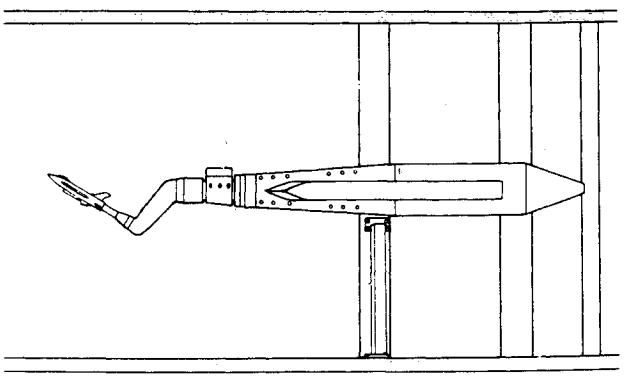

Fig. 12 Typical rotary rig.[15]

the static test. There is a definite similarity between the results in Fig. 14c and those for $Re = 1.5 \times 10^6$ in Fig. 9, indicating a similar support interference on the shed vortices from the model.

The change from the linear characteristics at $\alpha = 16$ deg (Fig. 14a) to the nonlinear ones at $\alpha = 24$ deg (Fig. 14b) have been determined to be caused by asymmetric flow separation on the wing, the separation being of a somewhat unsteady character. Looking at the cross-sectional fuselage geometry[17] (Fig. 15), one can suspect that flow separation from the fuselage interacted with the wing stall. The dynamic C_l results at $\alpha = 36$ deg indicate that this may have been the case (Fig. 16). If the Reynolds number is based upon the wing mean chord (which it appears to be) it is also approximately the Reynolds number based on the maximum cross-sectional width. With this in mind, one can compare the results[19] in Fig. 17 with those in Fig. 16. With the similarity in corner roundness and crossflow conditions, one might suspect that the critical Reynolds number was $Re \approx 10^6$ in both cases. The offset characteristics in Fig. 16 could then result from the moving-wall effects on the critical flow condition,[20] modified in the present case by the support interference.

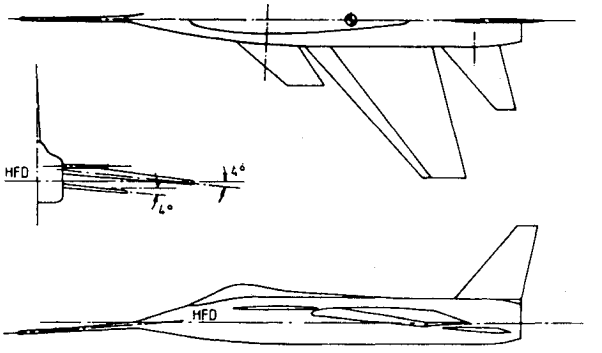

Fig. 15 HIRM Model.[17]

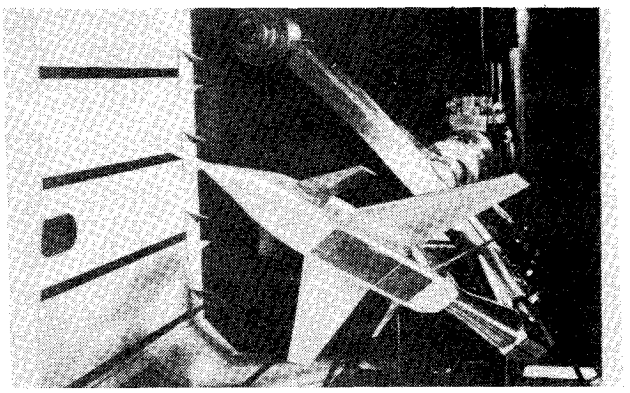

Fig. 13 HIRM model in rotating rig of 2.4×1.8-m wind tunnel.[17]

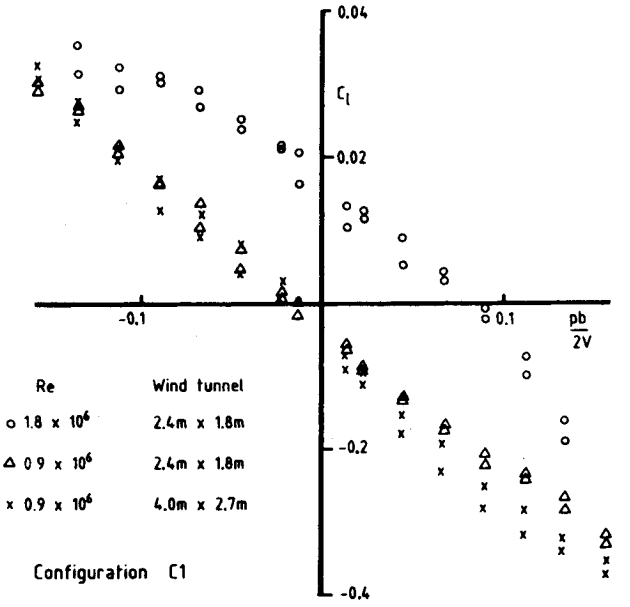

Fig. 16 Effect of Reynolds number on dynamic C_l characteristics of HIRM model at $M = 0.2$ and $\alpha = 36$ deg.[17]

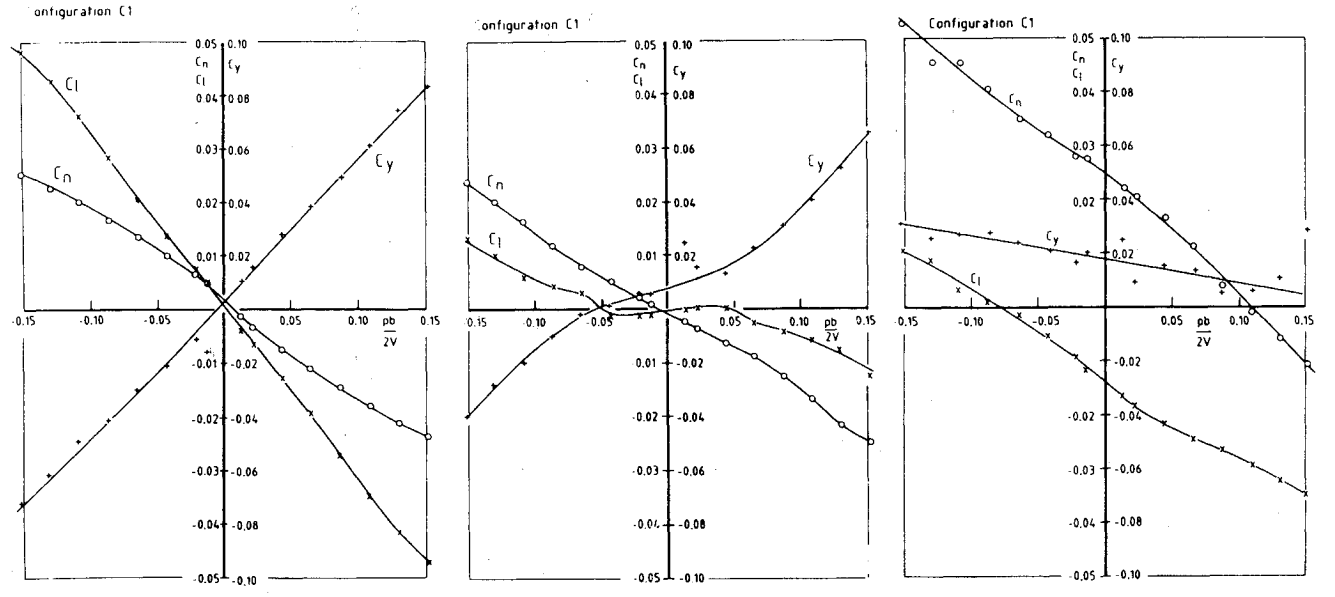

a) $\alpha = 16$ deg. b) $\alpha = 24$ deg. c) $\alpha = 40$ deg.

Fig. 14 Dynamic characteristics of the HIRM model at $M = 0.2$.[17]

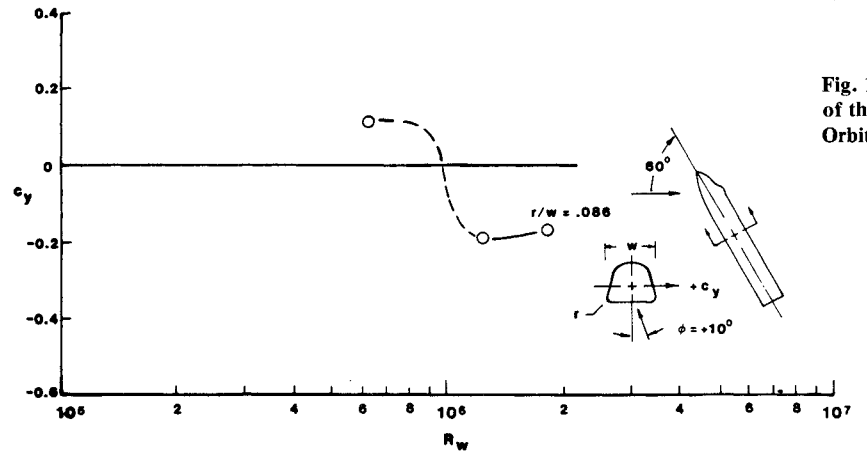

Fig. 17 Effect of Reynolds number on the side force of the fuselage of the straight-wing Space Shuttle Orbiter.[19]

Conclusions

A study of experimental results for advanced aircraft configurations obtained on rotary rigs at high angles of attack shows the following.

1) At angles of attack where asymmetric vortex shedding from a slender nose occurs, all of the different rig designs used appear to cause significant support interference.

2) A complicating factor in dynamic testing is the existing coupling between vehicle motion and the critical flow condition, as it is likely to be different in full-scale flight from what it is at the subscale test conditions usually existing in the rotary rig tests.

References

[1]Orlik-Rückemann, K.J., "Dynamic Stability Testing of Aircraft—Needs Versus Capabilities," *Progress in the Aerospace Sciences*, Vol. 16, No. 4, Pergamon, New York, 1975, pp. 431–447.

[2]Skow, A.M., Moore, W.A., and Lorincz, D.J., "Forebody Vortex Blowing—A Novel Control Concept to Enhance Departure/Spin Recovery Characteristics of Fighter and Trainer Aircraft," Paper 24, AGARD-CP-262, Sept. 1979.

[3]Ericsson, L.E. and Reding, J.P., "Review of Support Interference in Dynamic Tests," *AIAA Journal*, Vol. 21, Dec. 1983, pp. 1652–1666.

[4]Keener, E.R., Chapman, G.T., Cohen, L., and Taleghani, J., "Side Forces on Forebodies at High Angles of Attack and Mach Numbers from 0.1 to 0.7 Two Tangent Ogives, Paraboloid and Cone," NASA TMX-3438, Feb. 1977.

[5]Ericsson, L.E. and Reding, J.P., "Dynamics of Forebody Flow Separation and Associated Vortices," *Journal of Aircraft*, Vol. 22, April 1985, pp. 329–335.

[6]Ericsson, L.E. and Reding, J.P., "Review of Vortex-Induced Asymmetric Loads—Part I," Zeitschrift für Flugwissenschaften und Weltraumforschung, 5, 1981, Heft 3, pp. 162–174.

[7]Yanta, W. and Wardlaw, A., "Multi-Stable Vortex Pattern on Slender Circular Bodies at High Incidence," AIAA Paper 81-0006, Jan. 1981.

[8]Ericsson, L.E. and Reding, J.P., "Scaling Problems in Dynamic Tests of Aircraft-like Configurations," Paper 25, AGARD-CP-227, Feb. 1978.

[9]Malcolm, G.N., "Rotary-Balance Experiments on a Modern Fighter Aircraft Configuration at High Reynolds Numbers," AIAA Paper 85-1829, Aug. 1985.

[10]Ericsson, L.E. and Reding, J.P., "Alleviation of Vortex-Induced Asymmetric Loads," *Journal of Spacecraft and Rockets*, Vol. 17, Nov.-Dec. 1980, pp. 546–553.

[11]Ericsson, L.E. and Reding, J.P., "Asymmetric Vortex Shedding from Bodies of Revolution," Progress in Astronautics and Aeronautics, Vol. 104, edited by M.J. Hemsch and J.N. Nielsen, 1986, pp. 243–296.

[12]Reding, J.P. and Ericsson, L.E., "A Re-examination of the Maximum Normalized Vortex-Induced Side Force," *Journal of Spacecraft and Rockets*, Vol. 21, Sept.-Oct. 1984, pp. 433–440.

[13]Dietz, W.E. and Altstatt, M.C., "Exerimental Investigation of Support Interference on an Ogive-Cylinder at High Incidence," *Journal of Spacecraft and Rockets*, Vol. 16, March–April 1979, pp. 67–68.

[14]Hummel, D., "Untersuchungen über das Aufplatzen der Wirbel an schlanken Delta Flügeln," Zeitschrift für Flugwissenschaften, Vol. 13, Heft 5, 1965, pp. 158–168.

[15]Jermey, C. and Schiff, L.B., "Wind Tunnel Investigation of the Aerodynamic Characteristics of the Standard Dynamics Model in Coning Motion at Mach 0.6," AIAA Paper 85-1828, Aug. 1985.

[16]Ericsson, L.E. and Reding, J.P., "Dynamic Support Interference in High Alpha Testing," AIAA Paper 86-0760, March 1986.

[17]O'Leary, C. and Rowthorn, E.N., "New Rotary Rig at RAE and Experiments on HIRM," Paper 19, AGARD CP-386, May 1985.

[18]Ross, A.J. and Reid, G.E.A., "The Development of Mathematic Models for a High Incidence Research Model. Part I, Analysis of Static Aerodynamic Data," RAE Tech. Rept. 83037.

[19]Brownson, J.J., Graham, R.E., and Banducci, D., "Static Stability Characteristics of Manned Spacecraft Center Straight-Wing Space Shuttle Orbiter: Effect of Reynolds Number and Body Corner Radius at $M=0.5$," NASA TMX-62,054, 1971.

[20]Ericsson, L.E., "Aerodynamic Characteristics of Noncircular Bodies in Flat Spin and Coning Motions," *Journal of Aircraft*, Vol. 22, May 1985, pp. 387–392.